ISSN 1674-1056
http://cpb.iphy.ac.cn
http://iopscience.iop.org/cpb
中国物理 B
Chinese Physics
中国物理 Chinese Physics B

Characteristics of non-thermal AC arcs in multi-arc generator

Qifu Lin(林启富)[1,2], Yanjun Zhao(赵彦君)[1,2], Wenxue Duan(段文学)[1], Guohua Ni(倪国华)[1,3], Xinyue Jin(靳兴月)[1,2,3], Siyuan Sui(隋思源)[1,2], Hongbing Xie(谢洪兵)[1], Yuedong Meng(孟月东)[1]

Citation: Chin. Phys. B . 2019, 28(12): 125205 . **doi:** 10.1088/1674-1056/ab55ce
Journal homepage: http://cpb.iphy.ac.cn; http://iopscience.iop.org/cpb

What follows is a list of articles you may be interested in

Electric ignition energy evaluation and the energy distribution structure of energy released in electrostatic discharge process

Qingming Liu(刘庆明), Jinxiang Huang(黄金香), Huige Shao(邵惠阁), Yunming Zhang(张云明)
Chin. Phys. B . 2017, 26(10): 105202 . **doi:** 10.1088/1674-1056/26/10/105202

Characteristics of droplets ejected from liquid glycerol doped with carbon in laser ablation propulsion

Zhi-Yuan Zheng(郑志远), Si-Qi Zhang(张思齐), Tian Liang(梁田), Lu Gao(高禄), Hua Gao(高华), Zi-Li Zhang(张自力)
Chin. Phys. B . 2016, 25(4): 045204 . **doi:** 10.1088/1674-1056/25/4/045204

Current-voltage characteristics of hydrogen DC plasma torches with different sizes in an external axial magnetic field

Ma Jie, Wen Guang-Dong, Su Bao-Gen, Yang Yi-Wen, Ren Qi-Long
Chin. Phys. B . 2015, 24(6): 065205 . **doi:** 10.1088/1674-1056/24/6/065205

Experimental and modeling researches of dust particles in the HL-2A tokamak

Huang Zhi-Hui, Yan Long-Wen, Tomita Yukihiro, Feng Zhen, Cheng Jun, Hong Wen-Yu, Pan Yu-Dong, Yang Qing-Wei, Duan Xu-Ru, HL-2A Team
Chin. Phys. B . 2015, 24(2): 025204 . **doi:** 10.1088/1674-1056/24/2/025204

Charging and absorption characteristics of small particulates under alternative and electrostatic voltages in an electrostatic precipitator

Jiang Xue-Dong, Xu He, Wang Xin
Chin. Phys. B . 2014, 23(12): 125201 . **doi:** 10.1088/1674-1056/23/12/125201

Characteristics of non-thermal AC arcs in multi-arc generator*

Qifu Lin(林启富)[1,2], Yanjun Zhao(赵彦君)[1,2], Wenxue Duan(段文学)[1], Guohua Ni(倪国华)[1,3,†], Xinyue Jin(靳兴月)[1,2,3], Siyuan Sui(隋思源)[1,2], Hongbing Xie(谢洪兵)[1], and Yuedong Meng(孟月东)[1]

[1] *Institute of Plasma Physics, Chinese Academy of Sciences, Hefei* 230031, *China*
[2] *University of Science and Technology of China, Hefei* 230026, *China*
[3] *AnHui Province Key Laboratory of Medical Physics and Technology, Hefei* 230031, *China*

(Received 5 August 2019; revised manuscript received 6 November 2019; published online 29 November 2019)

To obtain large-volume non-thermal arc plasma (NTAP), a multiple NTAP generator with three pairs of electrodes has been developed. The arc plasma characteristics, including dynamic process, spatial distribution, and rotation velocity in the discharge zone, were investigated by high speed photograph and image processing methods. The results showed that the dynamic behaviors and spatial distribution of the arc plasma were strongly related to the electrode configuration. A swirl flow of multi-arc plasma was formed by adjusting the electrode configuration, and a steady luminance area was clearly observed in the center of the discharge zone. Moreover, the size of the luminance area increased by decreasing the gas flow rate. The electrical connection in series could be formed between/among these arc columns with their respective driving power supplies in the multi-arc dynamic evolution process. An approximately periodical process of acceleration and deceleration of the arc rotation velocity was observed in the multi-arc generator with swirl flow configuration. In general, the mean velocity of arc rotation was higher in the multi-arc generator with swirl flow configuration when a pair of electrodes driven by a power supply were opposite to each other rather than adjacent.

Keywords: characteristics, multiple arc plasma, multi-arc generator, non-thermal arc

PACS: 52.80.Mg, 52.70.–m, 52.50.Dg, 52.30.–q **DOI:** 10.1088/1674-1056/ab55ce

1. Introduction

Due to having the advantages of both thermal and cold plasmas, there has been an increasing interest in the warm plasma in recent years. Compared with the thermal and cold plasmas, it maintains moderate gas temperature (typically in the range of 1500–4000 K) and relative high concentration of radical species, which significantly improve the chemical reaction rate.[1,2] Therefore, the warm plasma has great application potentials in various fields, such as CH_4–CO_2 reforming,[3–7] combustion enhancement,[8–11] degradation of pollution,[12,13] material surface processing,[14–17] and material preparation.[18,19] The non-thermal arc discharge that produces non-thermal arc plasma (NTAP) is one of the fundamental methods for warm plasma generation, whose non-thermal characteristics are mainly realized by reducing the discharge current and/or keeping it in an unsteady-state. However, it has the disadvantages of arc plasma, such as small arc volume and arc instability.[1,19,20] Furthermore, the instability of NTAP (e.g., gliding arc plasma) is more severe compared with that of arc thermal plasma, since it periodically experiences the instability process from ignition to extinction, and its arc root has a wider range of motion.

Various types of NTAP generators have been developed to solve the whole or partial mentioned problems in recent years.[1,2,19–24] For enlarging the NTAP volume, one of the solution was to increase the sweeping area of the arc column in unit time. Many researchers, including Gangoli *et al.*,[1,2] Wang *et al.*,[19] and Zhu *et al.*[20] have investigated the effect of a magnetic field on arc, and a large time-average volume of NTAP was produced in a gliding arc plasma generator by applying an axial magnetic-field. Multi-arc plasma was an alternative method to enlarge the arc size by increasing the number of arcs per unit volume.[21,22] Tetsuro *et al.*[21] developed a multiple arc plasma generator with six knife-shaped electrodes, which was driven by a power supply with a six-phase transformer to form a six-phase 50 Hz alternating-current output. However, due to a single power supply used in the device, the multiple arcs did not exist inside the arc chamber at the same time. Another method that was used to enlarge the arc volume was glow-type discharge in NTAP by adjusting the experimental parameters, such as gas flow rate and discharge power, to meet the energetic balance between the input electrical energy and energy dissipation due to the convective cooling of the plasma column.[22–24] However, this process is difficult to control in practical industrial applications, because this type of discharge plasma is prone to change into shrinking arc under a minor disturbance.

In the present work, inspired by an invention patent of Xia *et al.*,[25] we developed a novel non-thermal multi-arc plasma generator with three pairs of electrodes to obtain large size

*Project supported by the National Natural Science Foundation of China (Grant Nos. 11875295 and 11535003), Provincial Science and Technology Major Project of Anhui Province, China (Grant No. 17030801035), and Key Program of 13th Five-year Plan, CASHIPS, China (Grant No. KP-2017-25).

†Corresponding author. E-mail: ghni@ipp.ac.cn

© 2019 Chinese Physical Society and IOP Publishing Ltd

NTAP, which was driven by three independent high-frequency power supplies. The high-speed image technique was employed to diagnose the dynamics and spatial distribution of the multi-arc plasma. The spatial distributions of arc plasma in the multi-arc generator were investigated by means of discharge image processing, which was combined with cross-correlation analysis to calculate the arc rotation velocity.

2. Experimental setup

Figure 1 illustrates a schematic diagram of the experimental setup, which consists of a multi-arc generator, three power supplies, a gas supply unit, an optical emission spectrometer, and a high-speed CCD camera. The multi-arc generator is mainly composed of six identical rod-type electrodes with their respective concentric ceramic bushings with inner diameter of 6 mm. These electrodes made of 1.50% lanthanated tungsten with diameter of 3 mm are symmetrically fixed in the same plane. The angle between any two adjacent electrodes is 60° and the distance between any two opposite electrode tips is 20 mm. These six electrodes are classified into three pairs, and each pair of electrodes is independently connected to the high-voltage outputs of an alternating current (AC) power supply. Air as the plasma working gas was evenly divided into six channels, and each channel was supplied to an electrode. The gas was introduced into the discharge zone with straight flow from each gap between the electrode and ceramic tube. The total gas flow rate was adjusted by a mass flow meter. The evolution of NTAP was captured by a high-speed camera (Photron Company, FASTCAM SA5 1000 K-M3) with a frame rate of 50000 frames per second (fps) and the exposure time of 0.02 milliseconds (ms). Each captured discharge image has a resolution of 512×368 pixels with a range of gray value from 0 to 65535.

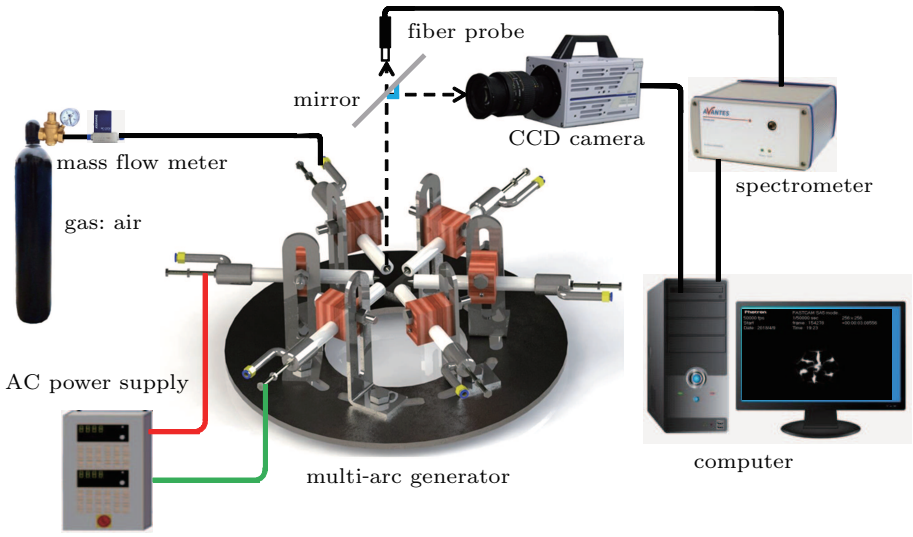


Fig. 1. Experimental setup for the multi-arc generator.

The main circuit schematic of the power supply used in the multi-arc generator is shown in Fig. 2. The circuit mainly consists of an electromagnetic interference (EMI) filter, a rectifier, a power factor correction (PFC), a half-bridge inverter, a resonant converter, a controller, and a high-frequency high-voltage transformer. The output of the power supply has the features of high voltage and low current with frequency of about 50 kHz, which is based on the resonant converter technology. The output terminals of the transformer (labeled as "A" and "A′") were connected to a pair of electrodes. The power supply has the maximum of no-load peak voltage of 15.0 kV with the power limitation of 1.0 kW. The discharge power was adjusted by the input voltage of the power supply. In the present work, the discharge voltage and current were simultaneously measured in order to investigate the electrical characteristic of the discharge plasma. It was found that there is a negative slope of the voltage–current curve for the arc discharge plasma. With an increase of the effective output current from 26.7 mA to 363.1 mA, the effective voltage decreased from 4.5 kV to 1.6 kV for each arc under the experimental condition of gas flow rate of 60 slm.

The properties of the multi-arc discharge, such as discharge area, fluctuation, and arc rotation velocity were investigated by data processing of the arc discharge image. The digital image processing technique[26,27] was used to calculate the discharge area. The image correlation analysis method was employed to determine the arc rotation velocity.

The gas temperature of the arc plasma was determined by using diatomic molecule OH ($A^2\Sigma \rightarrow X^2\Pi$, 0–0) spectral line fitting method.[28,29] The emission spectrum of the multi-arc discharge plasma was obtained in the center of the discharge zone by an AvaSpec-2048 spectrometer with a resolution of 0.1 nm in the spectral range from 200 nm to 1100 nm.

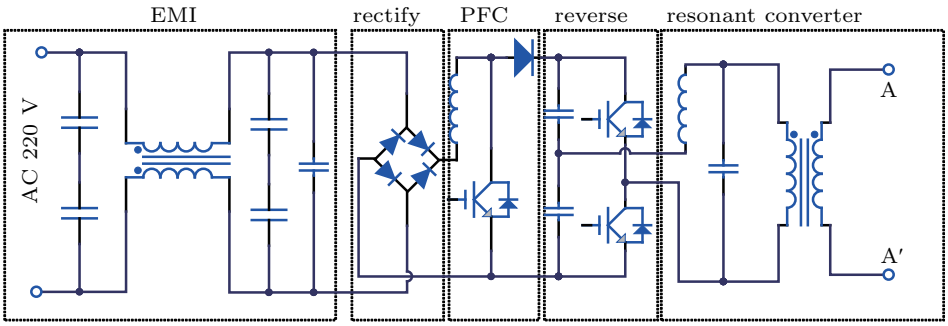


Fig. 2. The main circuit schematic of power supply used in the multi-arc generator.

3. Results and discussion

3.1. Flow field distribution

The gas flow has a great influence on the dynamic characteristics of the arc. In the experiment, due to the introduction of multiple airflows into the discharge zone, the distribution of the gas flow field was complicated. In order to evaluate the effect of the electrode configuration on the distribution of the flow field in the multi-arc generator, a series of numerical calculations using the software FLUENT were performed to obtain the specific parameters of its structure including the spacing and angle between the electrodes. Finally, two typical electrode configurations of the multi-arc generator were determined, and their geometric model and finite element mesh are shown in Fig. 3. The calculated region was evenly divided into a tetrahedron mesh with the mesh number of 1118481. This simplified model was mainly based on the following hypothesis: (i) The *k*-epsilon model was proposed to calculate the swirling flow. (ii) The gas flow in the multi-arc generator was supposed to be an incompressible turbulent fluid. (iii) The effect of gravity and arc discharge on the gas flow was neglected during the simulation.

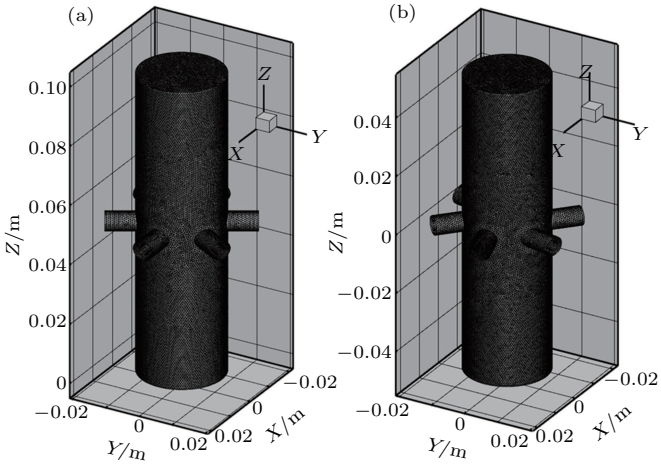


Fig. 3. Geometric model and finite element mesh of the multi-arc generator with (a) opposite-flow configuration and (b) swirl-flow configuration.

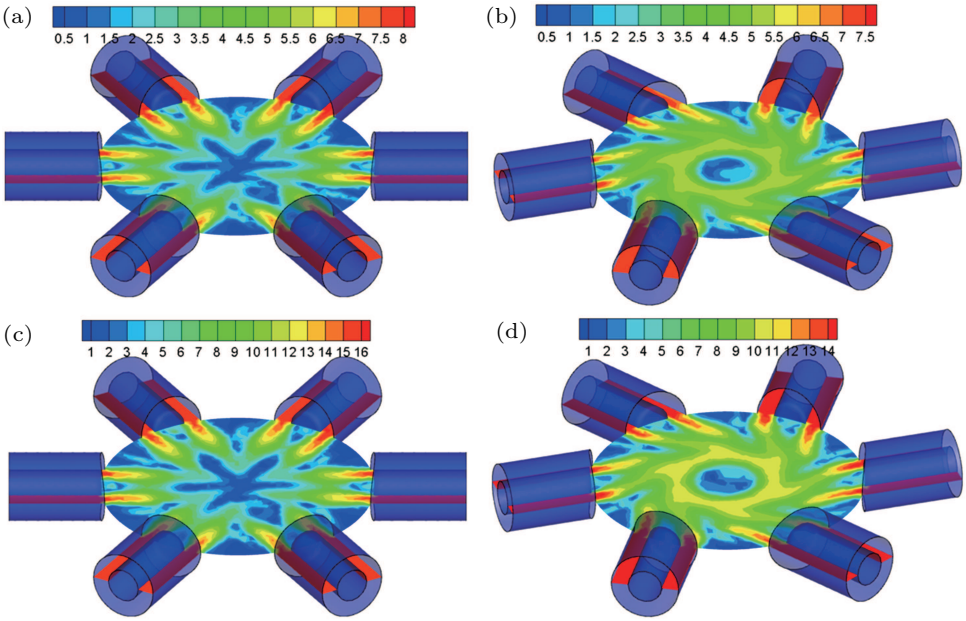


Fig. 4. Distribution of gas velocity field in the multi-arc generator with (a) opposite-flow configuration and (b) swirl-flow configuration under gas flow rate of 60 slm; (c) opposite-flow configuration and (d) swirl-flow configuration under gas flow rate of 120 slm.

Figure 4 shows the effect of the electrode configuration and gas flow rate on the distribution of the gas velocity field on the plane of $Z = 0$ mm in the multi-arc generator. It can be clearly seen that the opposite flow in the discharge zone was formed in the multi-arc generator with configuration of each pair of electrodes opposite to each other (it is termed as opposite-flow configuration here), in which all axes of the electrodes were intersected at the center of the discharge zone. There was a hexagram shape with a low velocity (< 2 m/s) region formed in the center of the discharge zone, as shown in Fig. 4(a), which was caused by the integrated offset of the gas flow velocities coming from six directions of the gas sources. The simulations also showed that the gas flow rate had a little effect on the flow field in the discharge zone, when the gas flow was increased from 60 slm to 120 slm, as shown in Figs. 4(a) and 4(c). Compared with the opposite-flow configuration, the swirl flow in the discharge zone was formed in the swirl-flow configuration, in which the extended lines of six electrode axis were tangent to a circle with diameter of 5 mm in the center of the discharge zone, as shown in Figs. 4(b) and 4(d). A rounded shape region with low gas flow rate (< 2 m/s) was formed in the center of the discharge zone of the multi-arc generator with the swirl-flow configuration. Furthermore, it can also be seen in Fig. 4 that the area with high gas flow rate (> 10 m/s) in the swirl-flow configuration was significantly larger than that in the opposite-flow configuration.

3.2. Typical spatial evolution of multiple arcs

According to the gas flow field analysis mentioned above, four typical electrode configurations for the multi-arc generator were determined by taking consideration of the connection order between the outputs of the power supply and the electrodes, which were denoted as configuration 1 (C_1), configuration 2 (C_2), configuration 3 (C_3), and configuration 4 (C_4), as shown in Fig. 5. In Fig. 5, the six electrodes were labeled with A, A′, B, B′, C, and C′, respectively, among which the capital letters stood for the output terminals of the three power supplies, respectively.

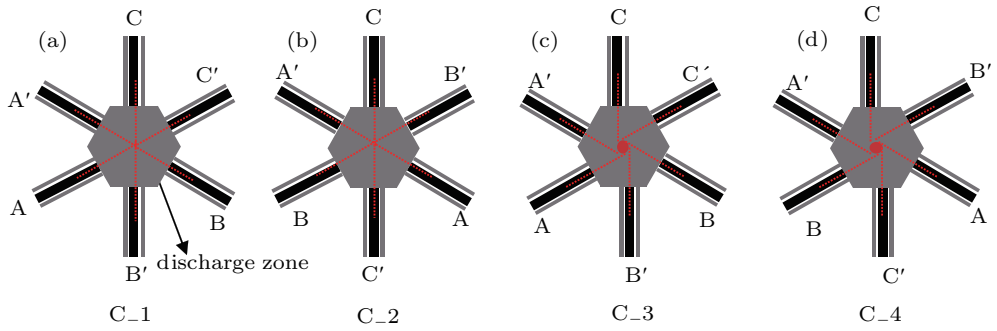


Fig. 5. The schematic of four types of electrode configurations in multi-arc generator, (a) configuration 1 (C_1), adjacent-electrode opposite-flow configuration, (b) configuration 2 (C_2), opposite-electrode opposite-flow configuration, (c) configuration 3 (C_3), adjacent-electrode swirl-flow configuration, (d) configuration 4 (C_4), opposite-electrodes swirl-flow configuration.

Figure 6 presents the typical discharge evolution in the multi-arc generator with C_1 under the experimental condition of gas flow rate of 60 slm and discharge power of 1.35 kW. The discharge states of multiple arcs exhibited marked periodic variations. Three arc columns were initially elongated towards the center of the discharge zone, which lasted about 1.2 ms. After 1.3 ms, two of them were close to each other in the center of the discharge zone, and finally connected together at 1.5 ms. At the moment of 1.6 ms, the three arc columns were all connected, as shown in Fig. 6, and this state lasted about 0.1 ms until one of the three arc columns became an independent one again. It took about 2.4 ms for multiple arcs from the connection establishment among the three arc columns to their complete disconnection. This duration may be mainly associated with the effect of gas drag force on arc column. The connection between/among different arc columns maybe result from their respective driving power supplies in series. Figure 7 indicates the schematic of series circuit of connection between/among different arcs with their respective driving power supplies. In the multi-arc generator with C_1, three pairs of adjacent-electrodes, such as A–A′, B–B′, and C–C′, were powered by three power supplies, respectively. The wide output range of the power supply allowed for driving complicated load, such as the series–parallel connection among multiple arcs. For instance, as shown in Fig. 7(a), besides forming a series loop between two arcs and two power supplies, part segment of arc column labeled as ‘a’ and ‘b’ acts as the bypass circuit, which means that a power supply maybe drive the load more than one arc. The magnitude of the no-load voltage of the power supply was about 15 kV, which was much higher than any arc voltage with the peak value lower than 5 kV. Therefore, the total output capacity of the three power supplies can easily satisfy the required voltage for the three arcs in series or more complicated series–parallel as shown in Fig. 7(b).

Figure 8 presents the typical successive discharge images in the multi-arc generator with C_2 under the experimental condition of gas flow rate of 60 slm and discharge power of

1.35 kW. Since the arc channels all passed through the center of the discharge zone, the three arc columns all connected and a luminance area was formed in the center of the discharge zone.

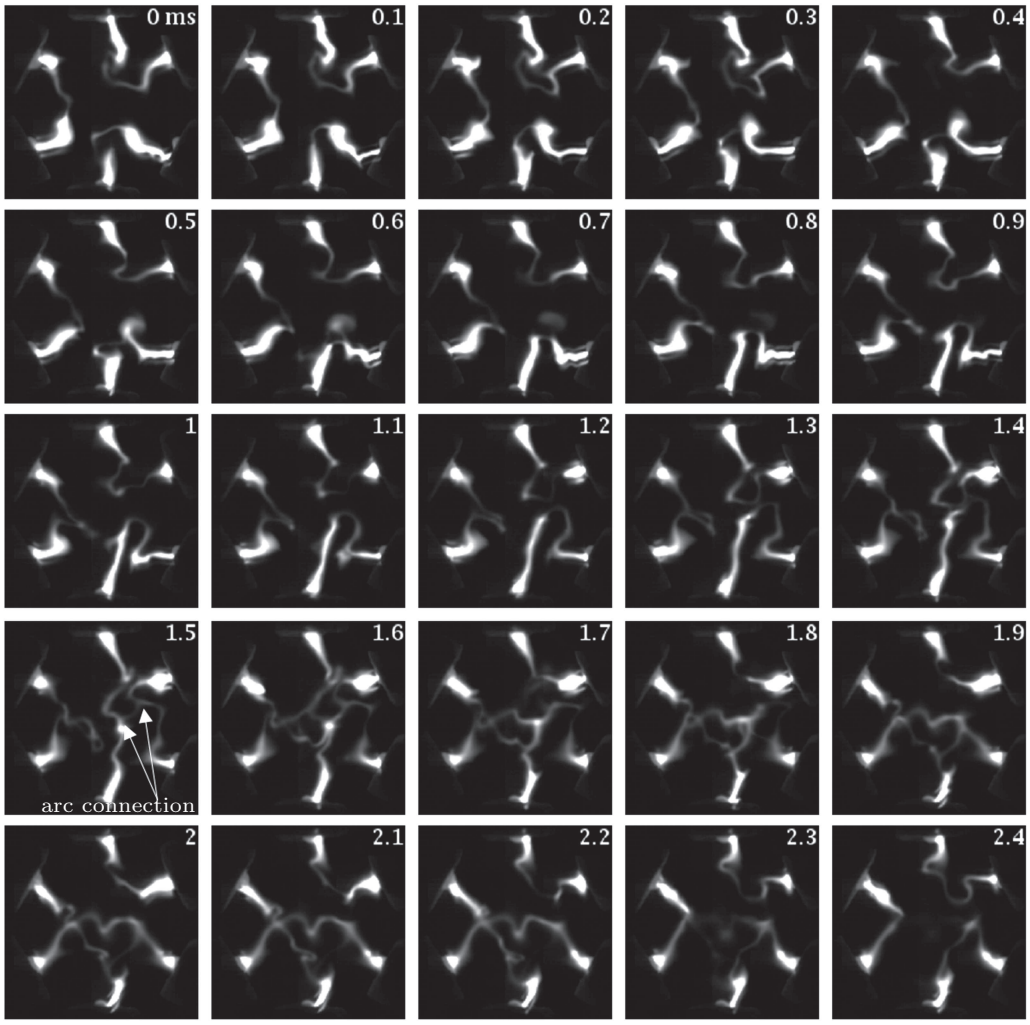


Fig. 6. Typical successive discharge images in multi-arc generator with C_1. The numbers give the time in millisecond.

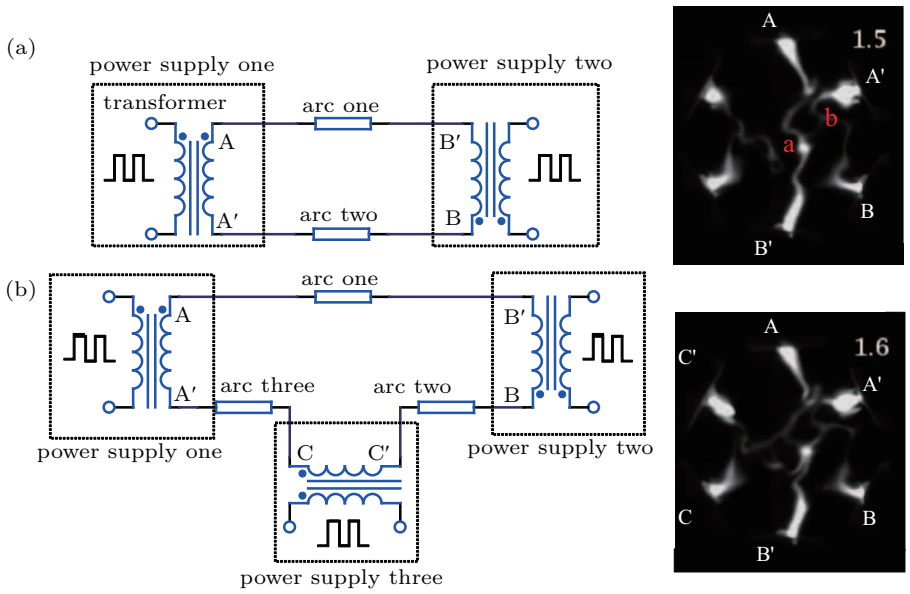


Fig. 7. The schematic for the connection order between power supplies and arc plasma in multi-arc generator, and the corresponding discharge image in Fig. 7; (a) two power supplies and two arcs, (b) three power supplies and three arcs.

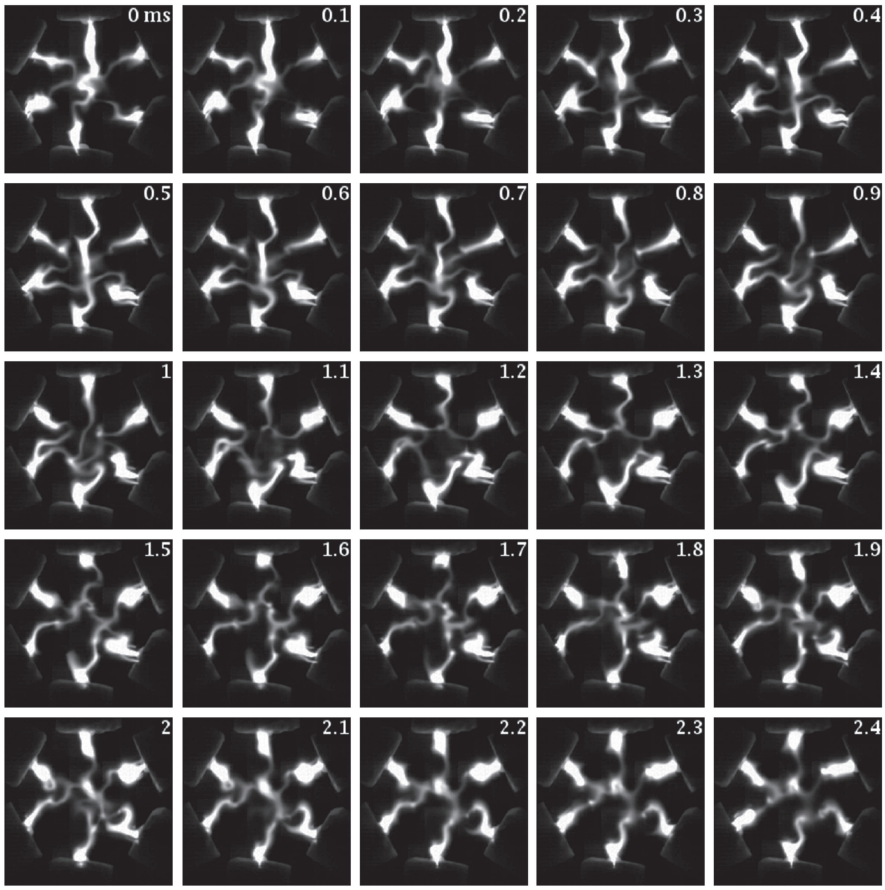


Fig. 8. Typical successive discharge images in multi-arc generator with C_2.

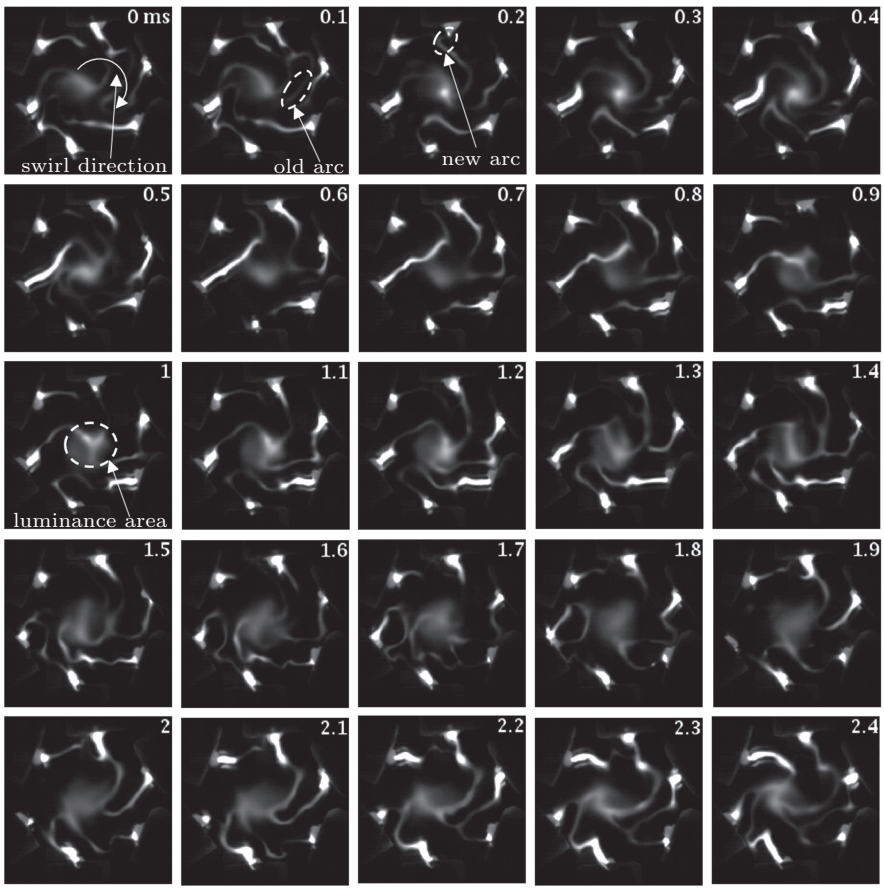


Fig. 9. Typical successive discharge images in multi-arc generator with C_3.

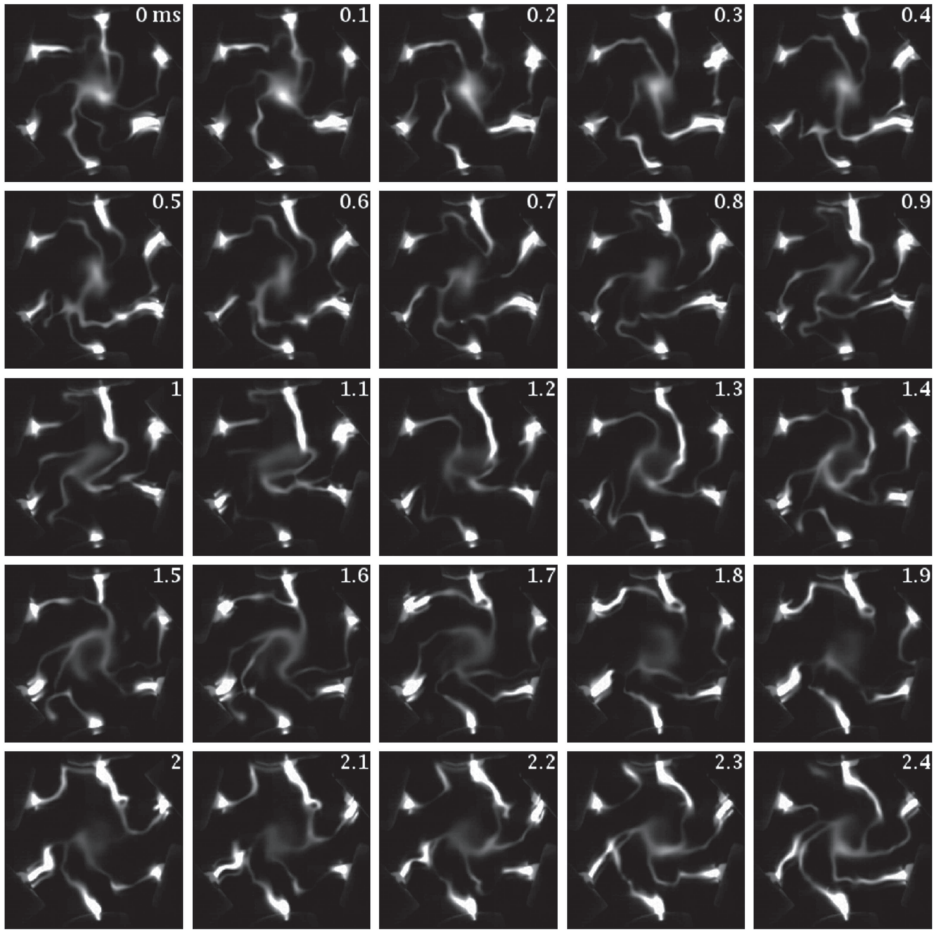


Fig. 10. Typical successive discharge images in multi-arc generator with C_4.

The typical discharge images in the multi-arc generator with C_3 and C_4 are shown in Figs. 9 and 10, respectively, under the same experimental condition. Due to the formation of swirling flow in the multi-arc generator with both C_3 and C_4, a relatively stable luminance area was formed in the center of the discharge zone. The multi-arc plasma appeared a regular rotation as a whole in the discharge zone. Each arc was periodically stretched along the direction of the swirl flow, and then replaced by a new arc, which was elongated again. Moreover, it was found that the frequency of new arc formation in C_3 was higher than that in C_4 by statistics analysis. The main reason of this phenomenon is due to the configuration of arc column in the discharge zone. The arc column was formed between two adjacent electrodes in C_3, while it was formed between two opposite electrodes in C_4. This means shorter distance and stronger electric field between two segments of an arc in C_3 than those in C_4. Therefore, the possibility of forming new arc channel between two segments of an arc column increased in C_3.

3.3. Arc spatial distribution and fluctuation

The spatial distribution of the arc is an important character for the multi-arc generator. Here, the parameter of the luminance ratio with different observing zone chosen was introduced to investigate the arc spatial distribution in the discharge zone, which is based on an assumption that the high-brightness region can be regard as arc covered or high temperature zone.[26,27] By analyzing and processing the discharge image, the parameters were obtained and the detail procedures are listed as follows:

(i) The origin discharge image (shown in Fig. 11(a)) was processed to delimit the discharge zone shown in Fig. 11(b).

(ii) Circular observing zones with diameters of 4 mm, 10 mm, 16 mm, and 20 mm were introduced, as shown in Fig. 11(c).

(iii) Converting the grayscale image into a binary image in black and white by setting a luminance threshold value of 7000, as shown Fig. 11(d).

(iv) Calculating the luminance area according to the grayscale value of each pixel in the observing zone.

(v) The luminance area ratio was obtained by a calculation of the luminance area divided by the area of the observing zone.

Figure 12 shows the effect of electrode configurations on the time-resolved luminance area ratio (TR-LAR) for different observing zones. It can be clearly seen that there were evident fluctuations of TR-LAR for all four electrode configurations, and the amplitudes of these fluctuations all decreased with the

increase of diameter of the observing zones. Since the high-brightness region can be assumed as arc covered or high temperature zone,[26,27] the fluctuation of TR-LAR indicated the fluctuation of average temperature in the observing zone or instability of arc sweeping through the observing zone. Moreover, the smaller the observing zone diameter was, the greater the differences among the TR-LAR of the four electrode configurations were, which implied that the arc plasma exhibited obviously different dynamic behaviors in the central area of the discharge zone. In Fig. 12(a), the TR-LAR of C_1 was relatively small compared with that of C_2, C_3, and C_4, which suggests that the gas temperature for C_1 may be relatively lower in the observing zone with diameter of 4 mm. This conclusion can be verified by comparing the time-averaged gas temperature in the center point of the discharge zone for the four electrode configurations. The gas temperatures in the center point of the discharge zone for C_1, C_2, C_3, and C_4 were 2600 K, 3000 K, 2800 K, and 4000 K, respectively, under the condition of discharge power of 1.35 kW and gas flow rate of 60 slm.

The effect of gas flow on the time-resolved luminance-area ratio in the multi-arc generator with C_4 in different observing zones is presented in Fig. 13 under the experimental condition of discharge power of 1.35 kW. It can be seen that the luminance area ratio at the gas flow rate of 60 slm had a high value (> 0.6) for most of the time when the diameter of the observing zone was 4 mm. In addition, it was observed that the luminance area ratio decreased with the gas flow rate increase for a fixed diameter of the observing zone. This phenomenon is mainly associated with the gas flow distribution surrounding the arc column. In the multi-arc generator, the gas flow velocity around the arc column, coming from six directions of gas sources, was enhanced with an increase of the gas flow rate, which results in a better cooling effect on the arc plasma and thus the reduced luminance area.

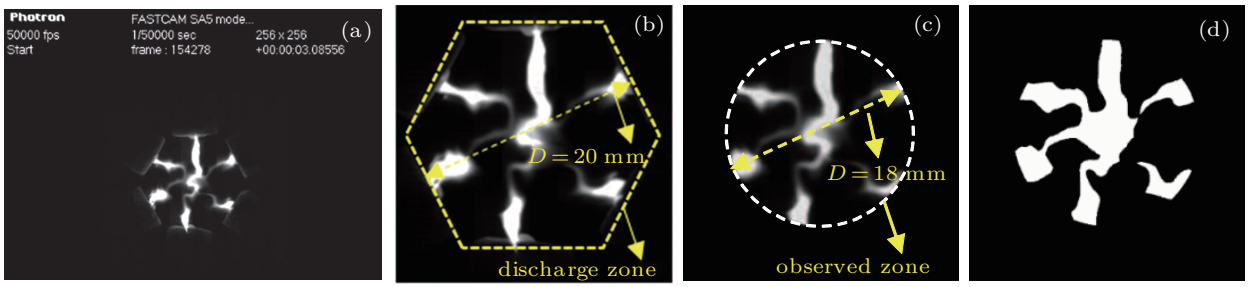


Fig. 11. Procedure for image analysis of luminance area generated by multiple arcs in C_2. (a) Origin discharge image, (b) delimit the discharge zone, (c) circular observing zones were introduced, (d) converting the grayscale image into binary image.

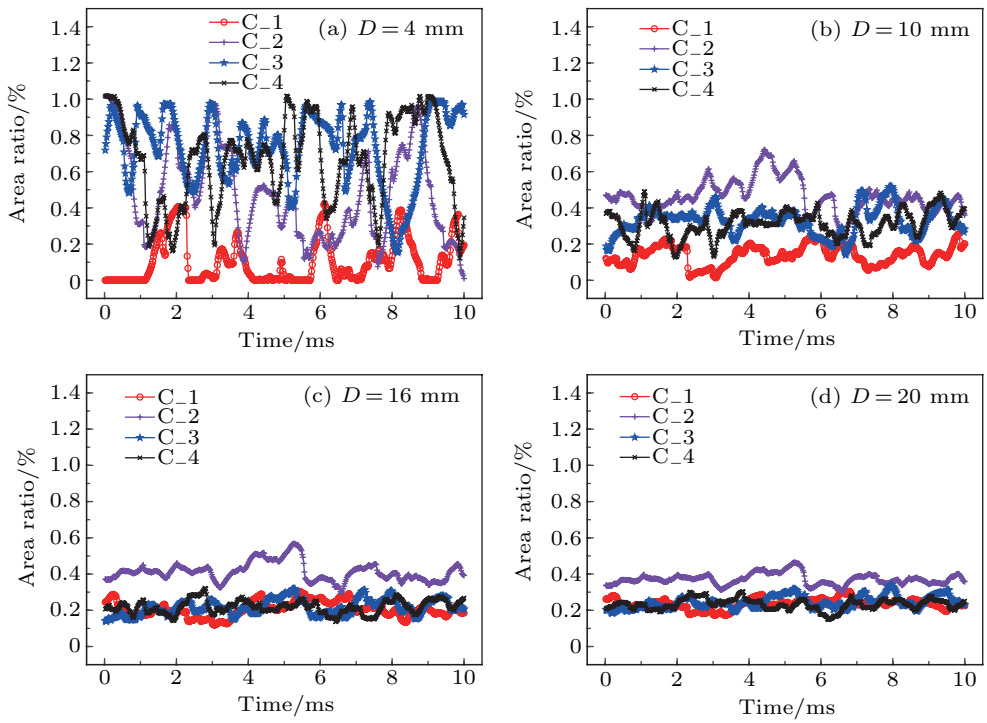


Fig. 12. The TR-LAR of four electrode configurations in different observing zones in the multi-arc generator. (a) $D = 4$ mm, (b) $D = 10$ mm, (c) $D = 16$ mm, and (d) $D = 20$ mm under C_1, C_2, C_3, C_4.

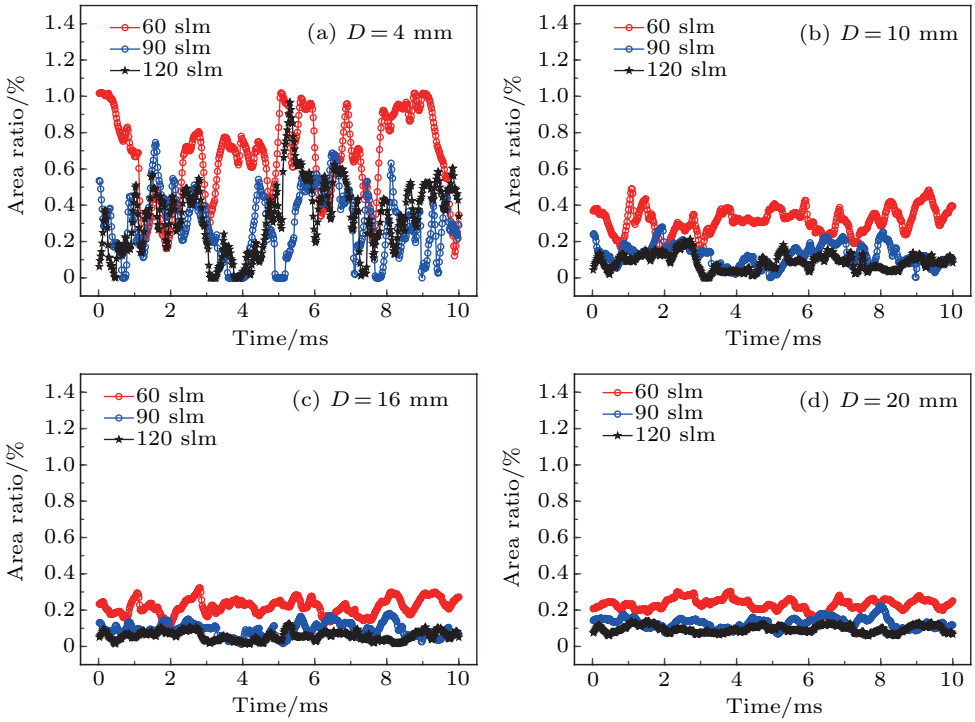


Fig. 13. The TR-LAR in different observing zones and gas flow rates in the multi-arc generator with C_4. (a) $D = 4$ mm, (b) $D = 10$ mm, (c) $D = 16$ mm, and (d) $D = 20$ mm under gas flow rates of 60 slm, 90 slm, 120 slm.

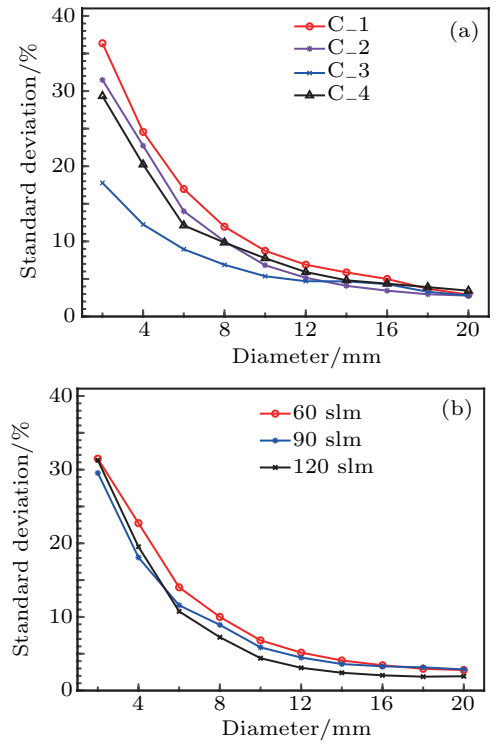


Fig. 14. The SD-LAR as a function of the diameter of the observing zone under (a) four electrode configurations, (b) different gas flow rates in the multi-arc generator with C_4.

As an effective tool to reflect the dispersion degree of signal, standard deviation was utilized to evaluate the stability of arc spatial distribution in the multi-arc generator. The standard deviation of luminance area ratio (SD-LAR) can be obtained according to the following equation:[30,31]

$$\tilde{I} = \frac{1}{N}\sum_{f=1}^{f=N}\sqrt{(I_f - \bar{I})^2}, \tag{1}$$

where $\tilde{I}$, N, f, I_f, and $\bar{I}$ represent the standard deviation, the total number of frames (500 frames selected in the present work), the frame number, the time-resolved luminance area ratio, and the time-averaged luminance area ratio, respectively.

The effect of electrode configurations and gas flow rate on the standard deviation of luminance area ratio is presented in Fig. 14. Among the four electrode configurations, the SD-LAR in C_3 is the smallest, which suggests that the stability of multi-arc plasma in C_3 was the best of all. Furthermore, the fluctuation in both C_3 and C_4 having a swirl flow in the discharge zone was lower than that in C_1 and C_2. The effect of gas flow rate on the SD-LAR in different observing zones for C_4 is shown Fig. 14(b). It can be concluded from the graph in Fig. 14(b) that the stability of arc luminance area in the observing zone was not sensitive to the gas flow rate.

3.4. Arc rotation velocity statistics

In the multi-arc generator with C_3 and C_4, the arc plasma rotated in the discharge zone due to the swirling field produced, which was caused by the electrode configuration. The arc movement is an important process that affects the heat and momentum transfer between the arc column and its surrounding media in its industrial application, and therefore the arc movement velocity is one of the key parameters for better understanding of this process. The high-speed photogra-

phy is an effective technical mean to determine this parameter, and the image processing method is one of the key links to obtain it. Zhu *et al.*[32] calculated the arc plasma velocity based on the nearest method to match a certain point of the arc column between two consecutive frames of images. By comparing and looking for the same position of arc column from two consecutive frames of images, the displacement of the arc motion is determined, and the arc column velocity can be obtained. However, this method cannot be used in our multi-arc system, because the boundary of each arc column was hard to be identified in the circumstance of multiple arcs confluence. Here, cross-correlation analysis based on probability statistics was introduced to calculate the arc rotation velocity (v_{arc}) in the multi-arc generator with C_3 and C_4, since the multiple arcs can be treated as a whole in this method. In the experiment, the multiple arcs as a whole rotated in the discharge zone, as a result, the spatial position of the arcs in the frame can be regarded as the corresponding position after the arcs in the previous frame rotates by an angle. This is the basis of using correlation analysis theory to obtain v_{arc}. Before the calculation of v_{arc}, several assumptions are listed as follows:

(i) Owing to the symmetry of the multi-arc generator, the differences among the rotation velocity magnitudes of multiple arcs were ignorable.

(ii) The v_{arc} was only calculated in the $Z = 0$ plane.

(iii) Compared with v_{arc}, the radial velocity was ignorable.

(iv) The fluctuation effect of gray-value distribution of discharge image on the cross-correlation coefficient was ignorable within the time step between two successive frame images.

In detail, the discharge images were processed as follows:

(i) Extract the discharge zone shown in Figs. 15(a) and 15(b) from the original discharge image.

(ii) Enlarge the image size by five times without distortion in order to improve the spatial resolution.

(iii) Extract the grayscale value of pixels along the circumference of the observing zone with diameters of 2 mm, 6 mm, 10 mm, and 14 mm from two successive frame images n and $n+1$.

(iv) Spread the gray value distribution along the circumference of the observing zone as shown in Figs. 15(c) and 15(d).

(v) The cross-correlation coefficient between two gray value distributions as a function of the arc displacement (ΔX) is shown in Figs. 15(e) and 15(f).

(vi) The v_{arc} was calculated by $v_{arc} = \Delta X/\Delta t$, where Δt is the time step, whose value was 0.02 ms, the time interval between two successive images.

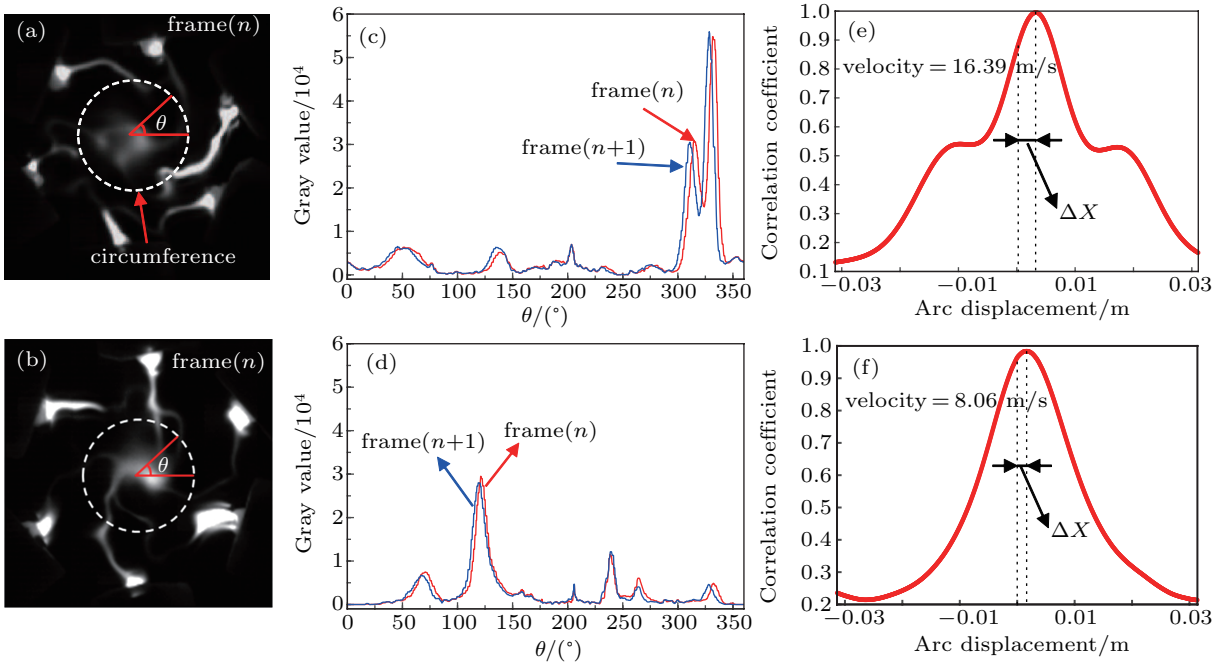


Fig. 15. Image analysis procedure of v_{arc} in multi-arc generator with different electrode configurations: (a), (c), (e) and (b), (d), (f) corresponding to C_3 and C_4, respectively. (a), (b) The original discharge images, (c), (d) extracted grayscale value of pixels along the circumference of the observing zone, (e), (f) the cross-correlation coefficient between two gray value distributions as a function of the arc displacement.

Figure 16 shows the time-resolved v_{arc} for C_3 at different diameters in the discharge zone under the experimental condition of gas flow rate of 60 slm and discharge power of 1.35 kW. It can be clearly seen that v_{arc} was almost zero at the diameter of 2 mm, where it is difficult to obtain the arc column displacement along the circumference of this circular. The possible reason is that the gray value distribution of arc plasma was relatively homogeneous, which maybe originates from relatively

uniform and diffuse arc plasma formed in this region. Besides, owing to the limited resolution of the CCD camera, the resolution of rotation rate calculated was 0.24 m/s. With the diameter increase, the value of v_{arc} firstly increased, and then decreased, as shown in Figs. 16(b)–16(d). It was noted that these v_{arc} changed with time over a wide range at a certain diameter, and the value of v_{arc} seems a random caused mainly by the turbulence effect of the interaction of multiple flows. In addition, it can be found that there was an implication of a process of acceleration and deceleration of v_{arc} in Figs. 16(b)–16(d). It should be noted that the v_{arc} calculated in above method is the magnitude of the average velocity of multiple arcs along the specified circumference in the present work, which is mainly from the elongation process of arc column. Therefore, this phenomenon can be interpreted that the differences exist between the gas flow rate v_{gas} and v_{arc}, and each arc had periodic motion that it was elongated and replaced by a new arc.

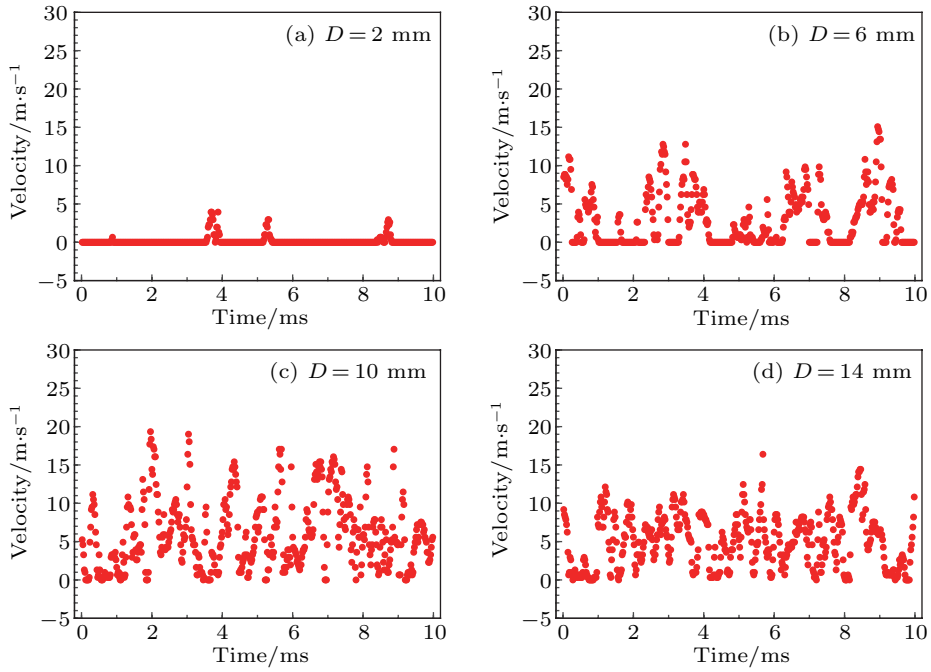


Fig. 16. The v_{arc} under different circles in multi-arc generator with C_3. (a) $D = 2$ mm, (b) $D = 6$ mm, (c) $D = 10$ mm, and (d) $D = 14$ mm.

The wave crest in the gray value distribution shown in Figs. 15(c) and 15(d) can be regarded as the zone covered by arc column. The arc motion in the multi-arc generator was mainly governed by the gas drag force, and the electromagnetic force on the arc column was ignored due to the low arc current operation. The gas drag force for arc rotation is given by the following equation:[1,2,33]

$$F_d = \frac{1}{2} C_d \rho (v_{gas} - v_{arc})^2 d, \tag{2}$$

where C_d, ρ, v_{gas}, and d correspond to the Reynolds number, density of plasma working gas, and equivalent diameter of arc column, respectively. Therefore, when multiple arcs had all just formed (v_{arc} is close to zero at the moment), it was dragged and its rotation motion was accelerated until it reached its maximum velocity. With a new arc generation and old one extinction due to arc distributaries, the weight of the new arc rotation velocity contribution to the magnitude of v_{arc} increases, which results in the v_{arc} decrease. A similar phenomenon occurred in C_4, as shown in Fig. 17.

In order to clearly distinguish the difference between the v_{arc} of C_3 and that of C_4, the mean v_{arc} was introduced to describe the arc time-average rotation rate, which was obtained by taking average of v_{arc} in 10 ms. The mean v_{arc} as a function of the diameter under different electrode configurations together with the simulation results is shown in Fig. 18(a) under the experimental condition of gas flow rate of 60 slm and discharge power of 1.35 kW. The variation trends for the mean v_{arc} as a function of the diameter between the experiment results and simulation results were similar, and both of the mean v_{arc} initially increased and then decreased with the diameter increase, and their maxima were at the diameter of around 8–10 mm. However, the mean v_{arc} of the experiment results was slightly higher than that of simulation at the diameter larger than 8 mm, which may be caused by the absence of the heating effect of plasma on enhancing the gas flow velocity during the simulation of the gas flow field distribution. Moreover, the mean v_{arc} of C_4 was higher than that of C_3, as shown in Fig. 18(a), which may be related to two factors, namely, the acceleration and accelerated time of arc motion. Firstly, it was found that the average acceleration of arc in C_4 was larger than that in C_3 when the derivative of v_{arc} (shown in Figs. 17 and 18) with respect to time was calculated. Sec-

ondly, the new arc column in C_3 was more easily formed in the discharge zone compared with that in C_4 as mentioned in Subsection 3.2, which resulted in the accelerated time of arc motion decrease.

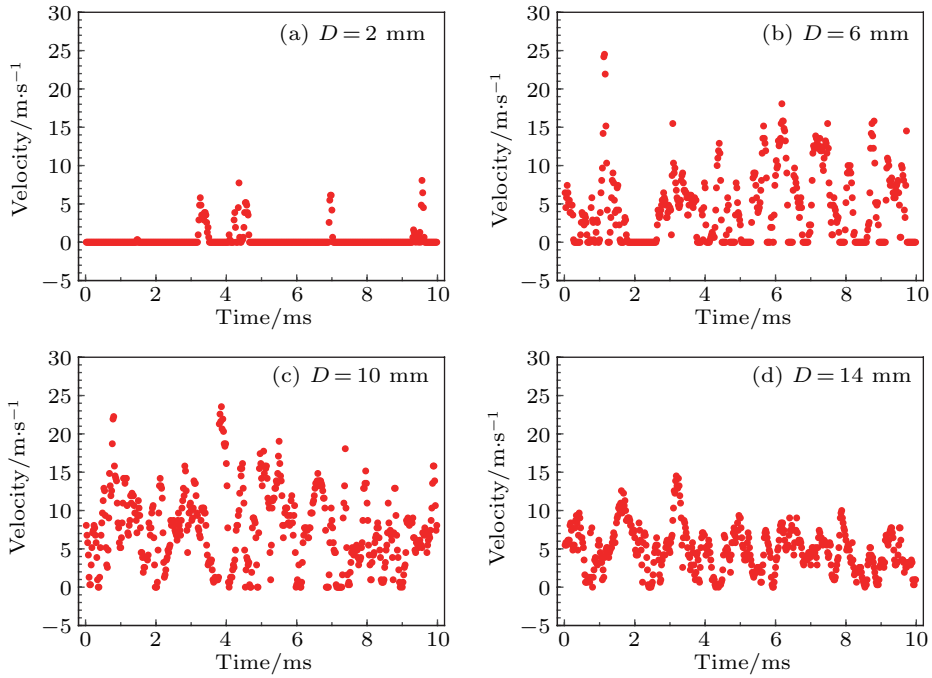


Fig. 17. The v_{arc} under different circles in multi-arc generator with C_4. (a) $D = 2$ mm, (b) $D = 6$ mm, (c) $D = 10$ mm, and (d) $D = 14$ mm.

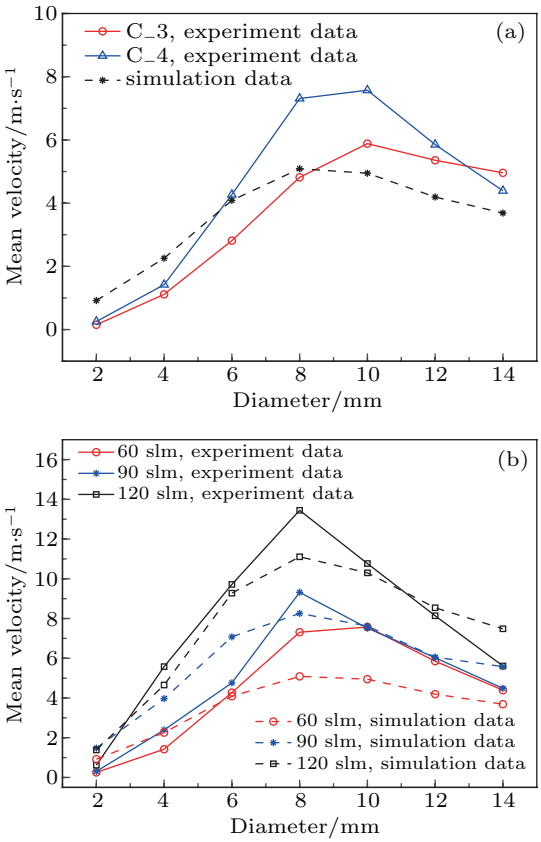


Fig. 18. Comparison of the simulation results and experiment results about the mean v_{arc} as a function of diameter under (a) different electrode configurations and (b) different gas flow rates in multi-arc generator with C_4.

The effect of the gas flow rate on the mean v_{arc} together with the simulation results is shown in Fig. 18(b) under the experimental condition of discharge power of 1.35 kW. The variation trends for the v_{arc} were also similar between the experiment and simulation results. An increase of gas flow rate led to a larger mean v_{arc} due to the larger gas drag force applied on the arc column. Therefore, higher v_{arc} can be achieved by adjusting electrode configuration and gas flow rate. Under the experimental condition of 120 slm gas flow rate and electrode configuration of C_4, the maximum of mean v_{arc} reached about 13.4 m/s at the circle with 8 mm in diameter, as shown in Fig. 18(b).

The errors brought by the experiment and this method are discussed as follows. First, the v_{arc} among multiple arcs may have small differences, which are mainly caused by the slight asymmetry of the multi-arc plasma generator. In our plasma generator, there are 1% differences among the six gas sources in our device and slight geometry flaws of electrodes themselves together with electrode configuration. Second, the maximum of cross-correlation coefficient ranges from 98% to 100%, which is mainly due to the fluctuation of arc plasma in the discharge zone. Third, it is difficult to obtain the accurate arc displacement utilizing cross correlation analysis method when the distribution of gray value of arc plasma is relatively homogeneous, e.g., at the diameter of 2 mm. Finally, the resolution of the CCD camera is another factor influencing the measurement accuracy. The area of each pixel in this study denotes the actual spatial resolution of 0.0576 mm^2, which means that the resolution of v_{arc} is 0.24 m/s.

4. Conclusion

In summary, the characteristics of AC arcs in the multi-arc generator with four electrode configurations have been investigated using high-speed photography, and an attempt has been made to measure the discharge area, the stability of discharge area, and the rotation velocity of multiple arcs. Several conclusions drawn from this paper are listed as follows.

(I) The spatial distribution of arc plasma, the arc plasma size, and its stability were strongly related to the electrode configuration. The opposite and swirl gas flows in the discharge zone could be obtained by adjusting the electrode position arrangement. In the electrode configuration with swirl flow, a luminance region in the center of the discharge zone was formed in C_3 and C_4. Moreover, the luminance region of arc plasma was more stable in C_3 and C_4 compared with that in C_1 and C_2. Besides, by adjusting the electrical connection order between electrodes and power supplies in the electrode configuration with swirl flow, the arc spatial distribution in C_3 was more stable than that in C_4.

(II) During the motion of multiple arcs, two or three arc columns maybe connect together in the discharge zone, and thus two or three arc columns together with their respective driving power supplies may be electrically in series operation.

(III) The v_{arc} approximately periodically changes in the multi-arc generator with swirl flow configuration. In general, the magnitude of v_{arc} can be enhanced by increasing the gas flow rate and using the electrode configuration with C_4. Under the experimental parameters of 120 slm gas flow rate and electrode configuration with C_4, the maximum mean of v_{arc} reached about 13.4 m/s.

References

[1] Gangoli S P, Gutsol A F and Fridman A A 2010 *Plasma Sources Sci. Technol.* **19** 065004

[2] Gangoli S P, Gutsol A F and Fridman A A 2010 *Plasma Sources Sci. Technol.* **19** 065003

[3] Liu J L, Park H W, Chung W J and Park D W 2016 *Plasma Chem. Plasma P.* **36** 437

[4] Lin Q F, Ni G H, Guo Q J, Wu W W, Li L, Zhao P, Xie H B and Meng Y D 2018 *IEEE. T. Plasma Sci.* **46** 2528

[5] Lu N, Sun D F, Xia Y, Shang K F, Wang B, Jiang N, Li J and Wu Y 2018 *Int. J. Hydrogen Energ.* **43** 13098

[6] Xia Y, Lu N, Wang B, Li J, Shang K F, Jiang N and Wu Y 2017 *Int. J. Hydrogen Energ.* **42** 22776

[7] Zhang H, Zhu F, Li X, Xu R, Li L, Yan J and Tu X 2019 *J. Hazard. Mater.* **369** 244

[8] Wu W W, Ni G H, Lin Q F, Guo Q J and Meng Y D 2015 *IEEE. T. Plasma Sci.* **43** 3979

[9] Wu W W, Ni G H, Guo Q J, Zhao P, Li L and Meng Y D 2016 *IEEE. T. Plasma Sci.* **44** 2952

[10] Larsson A, Adelow L, Elfsberg M and Hurtig T 2014 *IEEE. T. Plasma Sci.* **42** 3186

[11] Feng R, Li J, Wu Y, Zhu J J, Song X L and Li X P 2018 *Aerosp. Sci. Technol.* **79** 145

[12] Djakaou I S, Ghezzar R M, Zekri M E M, Abdelmalek F, Cavadias S and Ognier S 2015 *Plasma Chem. Plasma P.* **35** 143

[13] Krishna S, Maslani A, Izdebski T, Horakova M, Klementova S and Spatenka P 2016 *Chemosphere* **152** 47

[14] Feng Z B, Saeki N, Kuroki T, Tahara M and Okubo M 2012 *Appl. Phys. Lett.* **101** 041602

[15] Kusano Y, Sorensen B F, Andersen T L and Leipold F 2013 *J. Adhesion.* **89** 433

[16] Kusano Y, Sorensen B F, Andersen T L, Toftegaard H L, Leipold F, Salewski M, Sun Z, Zhu J, Li Z and Alden M 2013 *J. Phys. D: Appl. Phys.* **46** 135203

[17] Kusano Y, Zhu J J, Ehn A, Li Z S, Alden M, Salewski M, Leipold F, Bardenshtein A and Krebs N 2015 *Surf. Eng.* **31** 282

[18] Chaudhary K T, Ali J and Yupapin P P 2014 *Chin. Phys. B* **23** 035203

[19] Wang C, Lu Z S, Li D N, Xia W L and Xia W D 2018 *Plasma Chem. Plasma P.* **38** 1223

[20] Zhu F S, Zhang H, Li X D, Wu A J, Yan J H, Ni M J and Tu X 2018 *J. Phys. D: Appl. Phys.* **51** 105202

[21] Baba T, Takeuchi Y, Stryczewska H D and Aoqui S I 2012 *Przeglad Elektrotechniczny* **88** 86

[22] Zhu J J, Gao J L, Li Z S, Ehn A, Aldén M, Larsson A and Kusano Y 2014 *Appl. Phys. Lett.* **105** 234102

[23] Kong C D, Gao J L, Zhu J J, Ehn A, Aldén M and Li Z S 2017 *Phys. Plasmas.* **24** 093515

[24] Zhu J J, Gao J L, Ehn A, Aldén M, Larsson A, Kusano Y and Li Z S 2017 *Phys. Plasmas.* **24** 013514

[25] Xia W L, Wang C, Xia W D, Guo W K and Li C (C. N. Patent) 105682334 B [2018-11-20]

[26] Liu Y, Tanaka M, Choi S and Watanabe T 2014 *Int. J. Appl. Glass Sci.* **5** 443

[27] Yao Y, Yatsuda K, Watanabe T, Matsuura T and Yano T 2009 *Plasma Chem. Plasma P.* **29** 333

[28] Pellerin S, Cormier J M, Richard F, Musiol K and Chapelle J 1996 *J. Phys. D: Appl. Phys.* **29** 726

[29] Workman J M, Fleitz P A, Fannin H B, Caruso J A and Seliskar C J 1988 *Appl. Spectrosc.* **42** 96

[30] Chumak O, Kavka T and Hrabovsky M 2008 *IEEE. T. Plasma Sci.* **36** 1062

[31] Takana H, Jang J Y, Igawa J J, Nakajima T, Solonenko O P and Nishiyama H 2011 *J. Therm. Spray. Techn.* **20** 432

[32] Zhu J J, Gao J L, Ehn A, Alden M, Li Z, Moseev D, Kusano Y, Salewski M, Alpers A, Gritzmann P and Schwenk M 2015 *Appl. Phys. Lett.* **106** 044101

[33] McNall M and Coulombe S 2018 *J. Phys. D: Appl. Phys.* **51** 445203